Surpassing Challenges in Structured-Illumination Microscopy with FlexSIM

Emmanuel Soubies[1,*], Alejandro Nogueron[3], Florence Pelletier[4], Thomas Mangeat[2,5], Christophe Leterrier[4], Michael Unser[3], and Daniel Sage[3]

[1]IRIT, Université de Toulouse, CNRS, Toulouse, France
[2]Centre de Biologie Integrative, Toulouse, France
[3]Biomedical Imaging Group, EPFL, Lausanne, Switzerland
[4]Aix Marseille Université, CNRS, INP, NeuroCyto, Marseille, France
[5]LITC Core Facility, Université de Toulouse, CNRS, Toulouse, France

Abstract. Superresolution structured-illumination microscopy (SIM) is a powerful technique that allows one to surpass the diffraction limit by up to a factor two. Yet, its practical use is hampered by its sensitivity to imaging conditions which makes it prone to reconstruction artifacts. In this work, we present FlexSIM, a *flexible* SIM reconstruction method capable to handle highly challenging data. Specifically, we demonstrate the ability of FlexSIM to deal with the distortion of patterns, the high level of noise encountered in live imaging, as well as out-of-focus fluorescence. Moreover, we show that FlexSIM achieves state-of-the-art performance over a variety of open SIM datasets.

Super resolution | Structured-Illumination Microscopy | Image Reconstruction | Computational Imaging | Artifact Reduction | Patterns Estimation

Correspondence: *emmanuel.soubies@cnrs.fr*

1. Introduction

Since the seminal works of Heintzmann, Cremer [1] and Gustafsson [2], superresolution structured-illumination microscopy (SIM) has become increasingly popular [3–7]. Among superresolution fluorescence microscopy techniques [8–10], it is one of those that offer the best trade-off between spatial and temporal resolution [11–13]. Moreover, it does not require specific sample preparations, offers high photon efficiency, and supports multicolor imaging [3, 14, 15].

SIM is a prime example of *computational microscopy* that combines optics and numerical reconstruction so as to surpass the diffraction limit. Specifically, a set of structured illuminations is exploited to shift high-frequency components of the imaged sample within the bandpass of the optical system. Then, through dedicated algorithms, this high-frequency information is extracted from acquired data and used to generate an image with extended resolution. From a numerical standpoint, the importance and popularity of SIM can be measured by the growing number of reconstruction software packages [16]. These include, among open-source packages: SIMToolbox [17]; FairSIM [18]; OpenSIM [19]; Hessian-SIM [20]; DL-SIM [21]; HiFi-SIM [22]; ML-SIM [23]; JSFR-SIM [24]; Direct-SIM [25]; rDL-SIM [26]; or Open-3DSIM [27].

In conventional SIM, sinusoidal illumination patterns are used, which allows one to improve the resolution of wide-field microscopy by up to a factor two [1, 2]. Yet, several extensions of this conventional SIM setup have been proposed. They undertake to improve the resolution even further, to image thick samples, to reduce acquisition time, to simplify acquisition protocols, or to reduce background fluorescence [4–6]. For instance, a resolution improvement beyond a factor two is theoretically achievable if the fluorescence emission can be made to depend nonlinearly on the illumination [28–31]. Moreover, it has been shown that the use of random (speckle) illuminations improves the imaging of thick samples [32–35]. In another vein, SIM has been combined with total internal reflection fluorescence (TIRF) [36–38] or grazing incidence [39] illuminations. These limit the excitation to a few hundred nanometers above the coverslip, which strongly reduces out-of-focus fluorescence.

Unfortunately, SIM is particularly prone to reconstruction artifacts, which hinders its practical use. This has led some researchers to characterize and classify typical SIM artifacts [40–42]. Other researchers have dedicated their work to the development of i) detailed protocols for sample preparation [43] and system calibration [40, 44]; ii) numerical tools to assess image quality [45]; and iii) guidelines to best take advantage of reconstruction software packages [38, 40–42].

The quest for artifact-free SIM reconstruction is currently a very active area of research, as evidenced by the recent surge in numerical strategies such as the shaping of the reconstruction point-spread function (PSF) or optical transfer function (OTF) into an ideal form to reduce commonly seen artifacts [22, 46], the deployment of rolling reconstructions to mitigate motion artifacts in life imaging [20], the estimation and filtering of background fluorescence [47–49], the use of blind-reconstruction approaches [50–52], as well as the control of noise to remove structured-noise artifacts [53]. Finally, it is worth mentioning that deep neural networks have also been designed and trained to reduce artifacts in SIM reconstructions [54, 55].

This situation (along with the difficulties we experienced ourselves upon striving to significantly reduce reconstruction artifacts for challenging TIRF-SIM data using existing methods), motivated the development of FlexSIM. The promise of FlexSIM, for *flexible* SIM reconstruction, is to provide reliable SIM reconstructions for a variety of SIM data, going

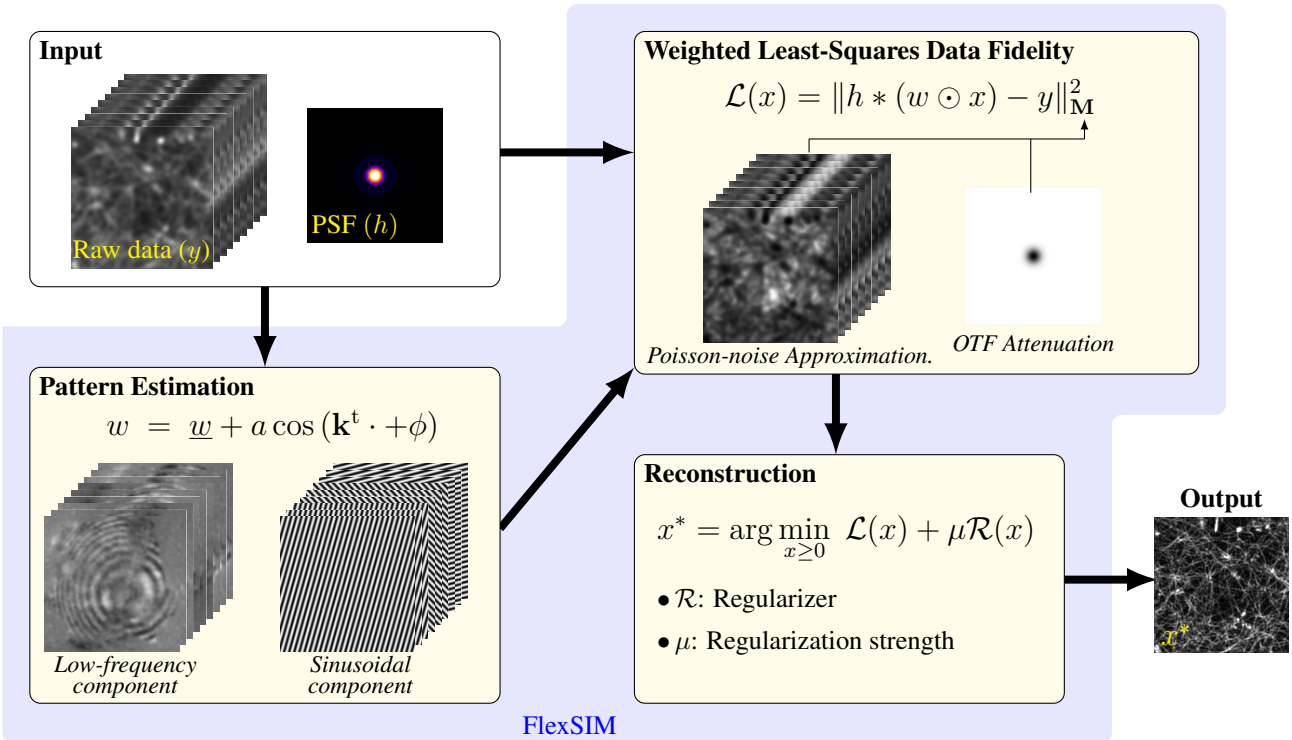

Fig. 1. Flowchart of FlexSIM. In addition to the ideal sinusoidal illuminations, low frequency pattern components $\underline{w}$ are estimated from raw data. For reconstruction, a weighted least-squares data-fidelity term is considered. The weighting operators $\mathbf{M}$ are built so as to account for both out-of-focus signal (similarly to OTF attenuation) and shot-noise. Finally, reconstruction can be performed with a variety of regularizers $\mathcal{R}$ and optimization algorithms.

from "ideal" ones acquired under standardized protocols and configurations, to ones obtained under more challenging settings and more prone to reconstruction artifacts.

2. Results

Foundations of FlexSIM

FlexSIM builds upon three pillars, highlighted in Figure 1.

1) Improved modelling. We propose the use of a more realistic model to represent the experimental illumination patterns. Specifically, we consider

$$w = \underline{w} + a\cos\left(\mathbf{k}^{\mathrm{t}} \cdot + \phi\right) \quad \textbf{(1)}$$

where $\underline{w}$ represents a low-frequency component (to be estimated from data) that refines the simple model of a purely sinusoidal SIM pattern with amplitude a, wave vector $\mathbf{k}$, and phase ϕ. This refinement turned out to be essential to treat challenging TIRF-SIM data, as shown in Figure 2. Then, reconstruction is performed using a weighted-least-squares data-fidelity term that allows us to account for both out-of-focus signal (similarly to OTF attenuation in standard Wiener-based reconstruction) and shot noise.

2) Auto-calibration of patterns. In FlexSIM, pattern phases and orientations are estimated through the optimization of the new criterion (4), which we tackle in a two-step procedure. The criterion is first evaluated on a grid of candidate parameters over which optimal ones are selected. This grid-based initialization, which can be efficiently performed through cross-correlation computations, somehow recovers the widespread approach of the seminal work [2], without the need to unmix frequency components. The proposed approach can thus work with uneven phase shifts. This initial estimation is then refined (off-the-grid) through a gradient descent over the proposed criterion. Regarding the estimation of the low-frequency component $\underline{w}$, we proposed in FlexSIM an efficient method to estimate it (one per SIM image) directly from the data (see *Methods*).

3) Advanced reconstruction. Lastly, FlexSIM benefits from the `GlobalBioIm` framework [56] which offers a variety of regularizers and optimization algorithms. By default, first-order Tikhonov, smoothed total-variation and good-roughness regularizers are proposed in FlexSIM. Optimization is performed with a quasi-Newton approach.

FlexSIM Deals with Pattern Distortions

An important feature of FlexSIM lies in its ability to cope with illumination patterns that exhibit a nonuniform low-frequency component, as described in (1). We report in Figure 2 an example of challenging TIRF-SIM data that are affected by such a degradation. Although not clearly visible on individual raw images (Figure S1.A), slowly varying con-

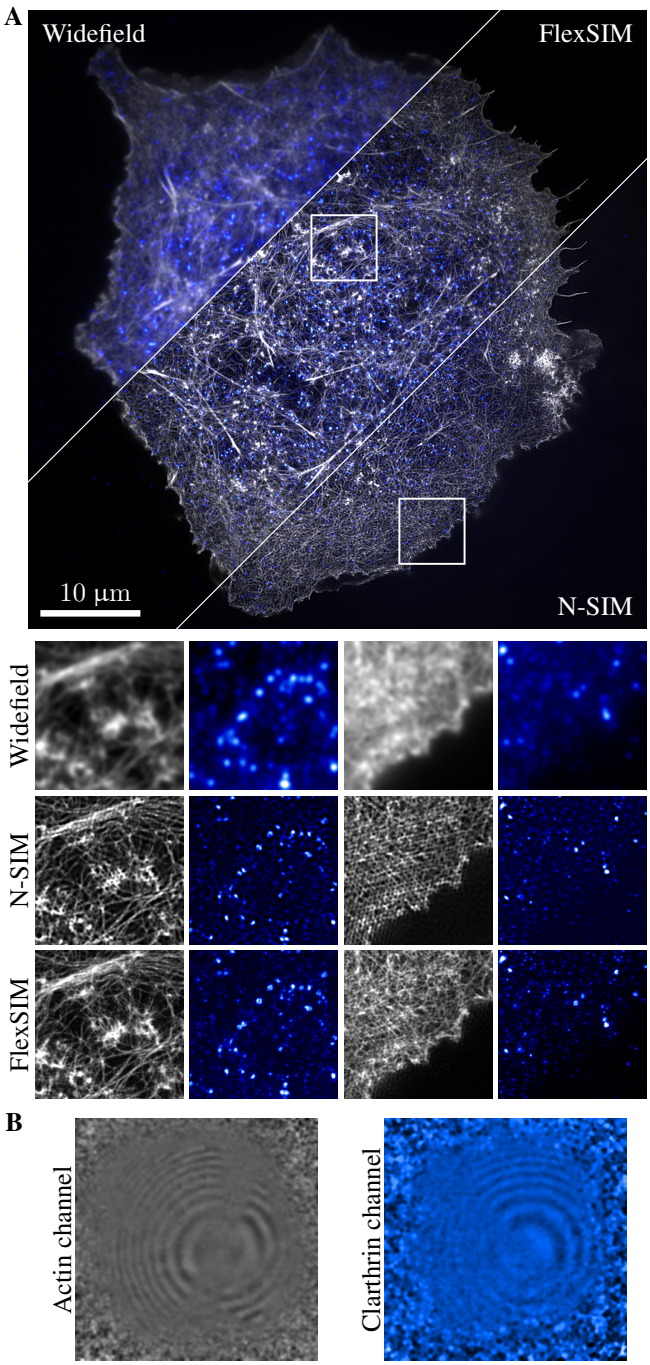

Fig. 2. FlexSIM reconstruction of challenging TIRF-SIM data. Actin network (gray) and clathrin (blue) in COS-7 cells imaged using the Nikon N-SIM-S system in TIRF-SIM mode. Raw images are of size (1024×1024) and reconstructions are (2048×2048). **A)** Comparisons of reconstructions obtained with FlexSIM and the N-SIM software. **B)** Low-frequency patterns components estimated by FlexSIM. Reconstructions of similar datasets are presented in Figures S3 and S4.

centric rings become apparent if one switches rapidly from one image to the next. The origin of these distortions is not entirely clear. They are most likely due to reflections from the TIRF edge configuration and, to date, cannot be systematically corrected on the optical side. Fortunately, these distortions are captured perfectly by the low-frequency component $\underline{w}$ estimated by FlexSIM (Figures 2.B and S1.B). Then, by incorporating these into the reconstruction process and by reconstructing each orientation separately, FlexSIM is able to produce well-contrasted and sharp images while standard SIM-reconstructions suffer from strong grid artifacts (Figure 2.A). Even the advanced OTF shaping proposed in HiFi-SIM [22] fails to avoid grid artifacts (Figure S2.B). It is worth mentioning that the grid artifacts reappear on FlexSIM reconstructions if we ignore $\underline{w}$ or if we do not consider each pattern orientation separately (Figure S2.A). These complementary experiments strengthen the relevance and importance of the new features proposed in FlexSIM.

We report in Figures S3 and S4 two additional reconstructions over the twelve similar cell samples we acquired on the same TIRF-SIM system. One observes that, when the estimated low-frequency pattern component $\underline{w}$ is homogeneous (clathrin channel in Figure S3.C, actin and clathrin channels in Figure S4.C), no artifacts are visible in the N-SIM reconstruction as well. This reinforces the fact that the presence of a nonuniform $\underline{w}$ is at the origin of the observed artifacts. Moreover, it is worth mentioning that, even when N-SIM reconstructions do not present artifacts, the corresponding FlexSIM reconstructions enjoy better contrast and dynamics.

FlexSIM Copes with Difficult Live Imaging Conditions

The TIRF-SIM data of Figure 2, which are already quite challenging, were acquired in fixed imaging conditions with high photon collection and low noise. In Figure 3, we consider even more challenging data by assessing the performance of FlexSIM in extreme live-imaging conditions. Precisely, we imaged a living neuron transfected with EGFP-β2-spectrin and clathrin-mCherry [57]. In addition to the presence of a low-frequency pattern component (Figure 3.C), these data present several other difficulties. In particular, they suffer from low photon collection (high noise) and strong illumination inhomogeneities that also vary according to the orientation of the pattern (Figure 3.A-B). Additionally, the imaged structure (neuron) only covers a small portion of the field of view. Lastly, marker strips spaced 190nm apart are present along the axon (horizontal structure). They are not visible on the widefield image and their spatial frequency is close to that of the grid artifacts.

The FlexSIM reconstruction of a temporal frame is presented in Figure 3.D. For comparison, the reconstruction obtained using the N-SIM software is depicted in the zooms of Figure 3.E. The full reconstructed temporal stack is provided in Video S1. While both methods are able to reveal the marker strips (Figure 3.E, left), they appear somehow distorted in one direction in the N-SIM reconstruction. We attribute this to the presence of grid artifacts intermingled with marker strips. Such grid artifacts are clearly

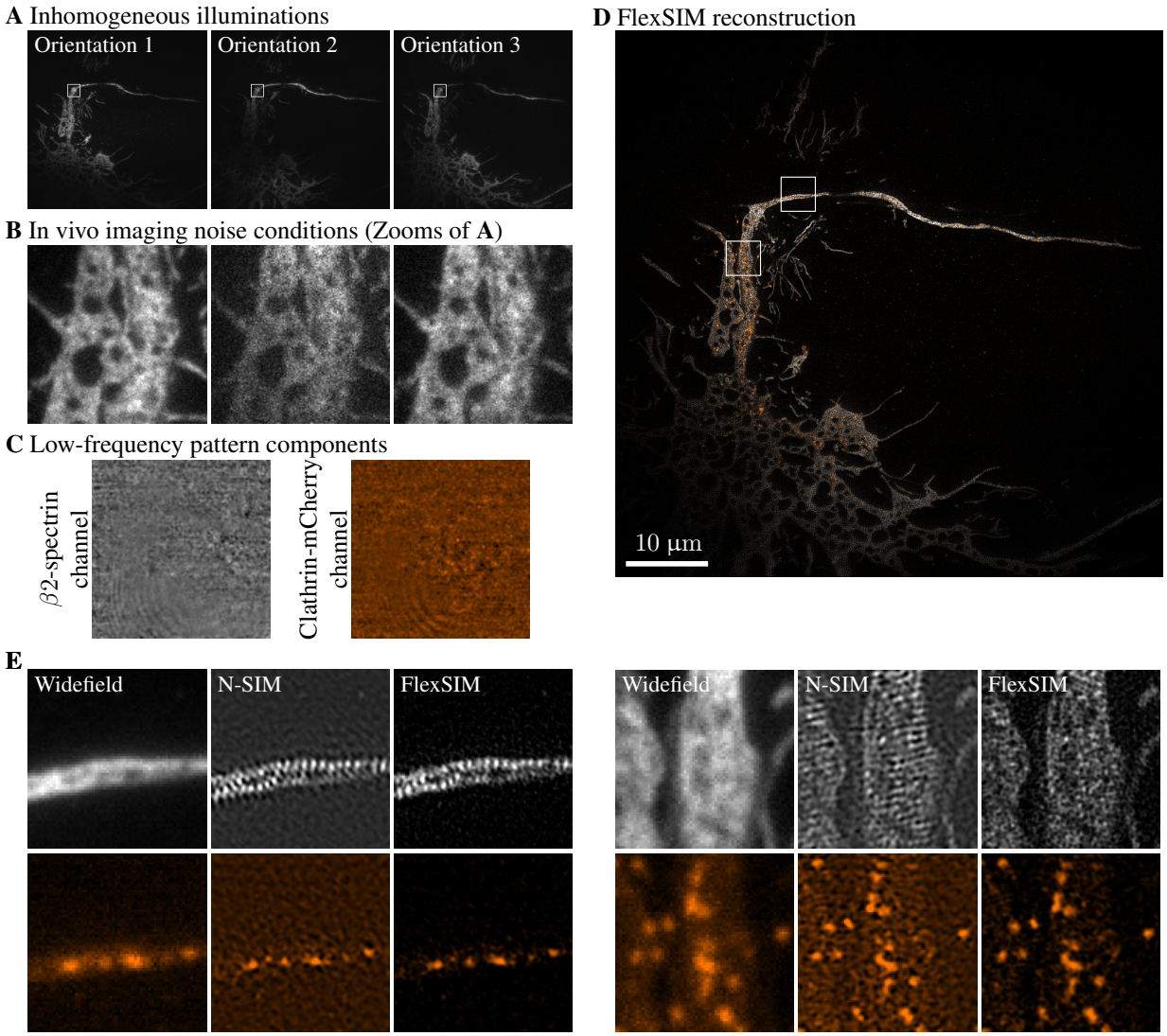

Fig. 3. FlexSIM in live TIRF-SIM imaging conditions. Clathrin-mCherry (orange) and $\beta 2$-spectrin expressed by a living neuron (gray). An 18-frame acquisition is performed with the Nikon N-SIM-S system in TIRF-SIM mode. Raw images are of size (1024×1024) and reconstructions are (2048×2048). **A**) Raw SIM data exhibit inhomogeneous illumination as well as **B**) high noise levels. **C**) Low-frequency pattern component estimated by FlexSIM. **D**) FlexSIM reconstruction (the full temporal stack available in Video S1). **E**) Zooms for the comparison of FlexSIM and N-SIM reconstructions.

visible in the dendrite region of the N-SIM reconstruction (Figure 3.E, right). Finally, FlexSIM has the remarkable ability to produce reconstructions free from residual background.

We also evaluated the performance of FlexSIM on data collected using a home-built TIRF-SIM system (Figure S5) [35]. To illustrate the difficulty of reconstructing these data, we were unable to estimate the frequencies and phases of patterns using FairSIM [18]. While Hifi-SIM [22] performed better for this task, the best reconstruction we managed to obtain with it suffers from important artifacts. In contrast, FlexSIM was able to properly estimate patterns parameters and to provide a clear reconstruction.

FlexSIM Achieves State-of-the-Art Performance on a Variety of Open SIM Datasets

To further demonstrate the capabilities of FlexSIM, we conducted in-depth comparisons with existing SIM reconstruction approaches. We considered twenty open 2D-SIM datasets sourced from seven publications and acquired with a diversity of SIM systems and configurations (see Table S1). Then, we benchmarked FlexSIM against methods developed in publications associated with each of these datasets. This represents seven different SIM reconstruction approaches ranging from standard Wiener-based reconstructions (and more advanced variants) all the way to deep-learning techniques. Accordingly, we could tune the parameters of each method as specified by the authors themselves, which ensures

a fair comparison.

A representative subset of the comparisons we made with the most recently published reconstruction approaches is presented in Figure 4. Complementary comparisons are provided in Figures S7–S9. One can see that FlexSIM performs as well as the best-in-class HiFi-SIM [22] and JSFR-SIM [24] methods while outperforming other algorithms. In particular, due to the proposed weighted-least-squares data-fidelity term, including an OTF attenuation strategy, FlexSIM strongly attenuates out-of-focus signal as well as typical associated artifacts. As with the TIRF-SIM data presented in the previous paragraphs, we can appreciate the ability of FlexSIM to systematically provide well-contrasted and crisp reconstructions across the large variety of data gathered in Table S1.

Finally, FlexSIM Matlab scripts for each dataset of Table S1 are publically available within the FlexSIM GitHub repository. These scripts automatically download the raw SIM data and set all FlexSIM parameters used to reproduce the results reported in the present paper for the sake of reproducibility. Beyond allowing us to assess FlexSIM performance, another motivation was to catalogue open 2D-SIM datasets and facilitate their access. We intend to update and enrich this collection of datasets as new ones are released.

3. Discussion

We have demonstrated experimentally the flexibility of FlexSIM to cope with a broad range of SIM data. We have included very challenging data for which no published method was known to attenuate the reconstruction artifacts as well as FlexSIM. To achieve this, we equipped FlexSIM with advanced features that include the modeling of a class of pattern distortions, the consideration of shot noise, and the attenuation of out-of-focus fluorescence. The price to pay, however, is the need for an iterative reconstruction scheme which is slower than direct Wiener-based inversion. Typically, our reconstruction of the (2048×2048) TIRF-SIM images (e.g., Figures 2 and 3) is obtained in about six minutes on a Dell Latitude computer (Intel Core i7-8650U CPU 1.90GHz × 8) with parallel computing. The reconstruction time for smaller (1024×1024) images ranges between 1 to 3 min, depending on the number of iterations. We expect that the computational time of FlexSIM can be markedly decreased if one deploys GPU computation [59].

We acquired new insights while developing FlexSIM. In particular, the estimation of pattern frequencies and phases through the formalization of this problem as the minimization of a suitable criteria helped us to clarify certain assumptions that had remained implicit to this day. This has allowed us to integrate them properly within the problem (see Figure S10). Moreover, we have highlighted the benefit of our local off-the-grid refinement over an oversampling of the data to achieve subpixel wave vector localization (see Figure S11).

Finally, FlexSIM is available as a documented open-source code with a pool of example scripts that allow one to reproduce the reconstructions reported in this work for each dataset of Table S1. Users can also deploy FlexSIM easily on any other dataset by filling a single file collecting every required parameter.

4. Methods

We provide in Sections A and B the methodological details behind each step of the FlexSIM pipeline (Figure 1).

Notations. We write vectors as bold lowercase letters (e.g., $\mathbf{x}$, $\mathbf{k}$) and their transpose as $\mathbf{x}^{\mathrm{t}}$, $\mathbf{k}^{\mathrm{t}}$. The mth component of a vector $\mathbf{x} \in \mathbb{R}^M$ is x_m. We denote the Fourier transform of a function v (lowercase) by it uppercase counterpart V. The symbols $*$ and $\odot$ stand for convolution and pointwise multiplication operations, respectively. The complex conjugate of $a \in \mathbb{C}$ is denoted $\bar{a}$. We denote by $\langle \cdot, \cdot \rangle$ the standard Hermitian inner product, the conjugation being applied to the first argument by convention.

A. Pattern Estimation Module

A.1. The Art of Pattern Estimation. An accurate pattern estimation is essential to limit reconstruction artifacts. The vast majority of existing approaches work under the assumption that the spatial phases shifts of patterns sharing the same orientation are regularly spaced within $[0, 2\pi]$. This allows for a simple separation of the Fourier components contained in the raw SIM images from the sole knowledge of relative phases. Then, the maximization of the cross-correlation between these extracted Fourier components leads one to estimate the orientations of the patterns, as well as their frequencies and phase offsets [2, 18, 60]. While this strategy proved to be very efficient to estimate pattern orientations and frequencies, it may not provide a sufficiently accurate estimation of phases. As such, several works have been dedicated to phase estimation, assuming that orientations and frequencies are known and that phases are not necessarily regularly spaced [61–64]. Finally, there exist alternative approaches that exploit either Prony's annihilation property [65], or the low-rank nature [58] of SIM illuminations.

A.2. Patterns Estimation with FlexSIM. Let $\{w_m\}_{m=1}^M$ be M illumination patterns having the same orientation but different phases $\{\phi_m\}_{m=1}^M$. In conventional 2D-SIM, patterns are generated from the interference between two beams and are modeled as

$$w_m(\mathbf{x}) = 1 + a_m \cos\left(\mathbf{k}^{\mathrm{t}}\mathbf{x} + \phi_m\right), \tag{2}$$

where $a_m > 0$ is the modulation contrast, $\mathbf{x} \in \mathbb{R}^2$ the spatial variable, and $\mathbf{k} \in \mathbb{R}^2$ the modulation light wave vector. The associated (noiseless) SIM data $\{v_m\}_{m=1}^M$ are then given by

$$\begin{aligned} v_m &= h * (w_m \odot u) \\ &= h * u + a_m h * \left(\cos\left(\mathbf{k}^{\mathrm{t}} \cdot + \phi_m\right) \odot u\right), \end{aligned} \tag{3}$$

where u represents the sample and h the PSF of the optical system. In the sequel, we denote by $\tilde{v} = h * u$ the widefield image, which we assume to be accessible. When the phases are equally spaced, we have that $\tilde{v} = \sum_{m=1}^M v_m$. Otherwise,

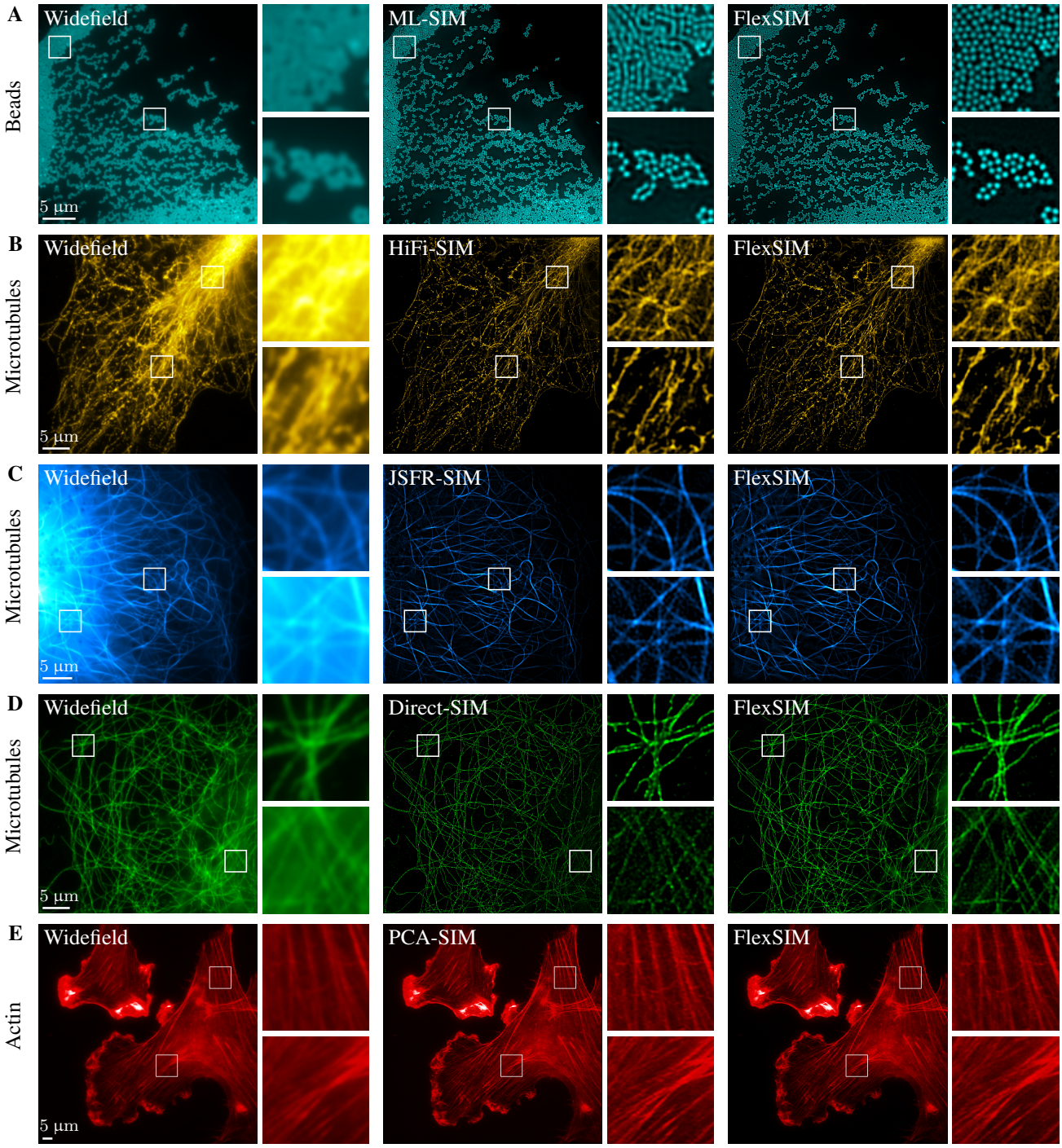

Fig. 4. Benchmarking FlexSIM against existing software on their own datasets. A subset of the 20 open 2D-SIM datasets reported in Table S1. From left to right, columns correspond to the widefield image, the comparative reconstruction and the FlexSIM reconstruction. Other comparisons are provided in Figures S7–S9. Note that PCA-SIM [58] in **E** is a method that uses principal component analysis for the estimation of patterns parameters. The reconstruction is then performed using HiFi-SIM [22].

the widefield image can be acquired together with the SIM stack.

To drop the dependence on the sample u, which is unknown, we make the approximation that $u \approx \tilde{v}$. Then, pattern parameters can be estimated through the minimization with respect to $\mathbf{a}$, $\boldsymbol{\phi}$, and $\mathbf{k}$ of the criterion

$$\mathcal{J}(\mathbf{a}, \boldsymbol{\phi}, \mathbf{k}) = \sum_{m=1}^{M} \| a_m h * \left(\cos\left(\mathbf{k}^{\mathrm{t}} \cdot + \phi_m\right) \odot \tilde{v}\right) - g * \tilde{v}_m \|_2^2, \tag{4}$$

where $\boldsymbol{\phi} \in [0, 2\pi)^M$, $\mathbf{a} \in \mathbb{R}_{>0}^M$, and g is a filter introduced to mitigate the effect of the approximation $u \approx \tilde{v}$. It is related to the idea of notch filtering used in other works [22] and illustrated in Figure S10. Finally, $\tilde{v}_m = (v_m - \tilde{v})$ corresponds to the mth raw SIM data without the widefield component. In practice, to account for scaling factors, we compute $\tilde{v}_m := (\alpha_m v_m - \tilde{v})$ for α_m that minimizes the error $\|D \odot (\widetilde{V} - \alpha_m \widetilde{V}_m)\|_2^2$, that is $\alpha_m = \langle D \odot \widetilde{V}, D \odot \widetilde{V}_m \rangle / \|D \odot \widetilde{V}_m\|_2^2$. Here, D is a mask that allows us to compute the error between low frequencies only (e.g., a disk in Fourier).

The function $\mathcal{J}$ is highly nonconvex, making its minimization a challenging task. As such, we propose a two-step procedure.

1. *Grid-Based Initialization.* The idea here is to consider an approximation of $\mathcal{J}$ that can be efficiently evaluated on a grid $\mathcal{K} = \{\mathbf{k}_q\}_{q=1}^{Q}$ of candidate wave vectors, and then select $\mathbf{k}_{\text{init}} = \min_{\mathbf{k} \in \mathcal{K}} \mathcal{J}(\mathbf{k}) \in \mathcal{K}$. We refer the reader to Supplementary Note 1 for a full derivation. Similar to standard pattern-estimation approaches [2, 62], the proposed grid-based initialization relies on cross-correlation computations. Yet, it does not require us to first unmix the frequency components. The advantage is that it can work with uneven phase shifts in a non-iterative way. The main computational cost lies in the computation of M cross-correlation maps. In that respect, it has links with the method proposed in [63].

2. *Local Off-the-Grid Refinement.* The goal here is to improve the initial estimation through a local optimization of $\mathcal{J}$. This allows us to obtain an estimate of the wave vector that is not constrained to be on the grid $\mathcal{K}$ used at initialization. Moreover, the proposed local refinement deals with the exact function $\mathcal{J}$. It proceeds by alternating between a minimization of $\mathcal{J}$ with respect at first to $(\mathbf{a}, \boldsymbol{\phi})$, and then $\mathbf{k}$. For the minimization over $(\mathbf{a}, \boldsymbol{\phi})$, we recast the problem as the resolution of M (2×2) systems of linear equations that can be solved efficiently. Regarding the minimization of $\mathcal{J}$ over $\mathbf{k}$, we derive a closed-form expression of the gradient and deploy gradient-descent steps. Full details are provided in Supplementary Note 1.

Numerical Validation. We report in Figure S11 a series of numerical experiments over simulated data. As expected, we observe that errors decrease when the level of noise decrease, that is when the maximal expected number of photons (MEP) increases. For all noise levels, the wave vector is estimated with a precision that is beyond a tenth of pixel and reaches a hundredth of pixel for low noise levels. For the estimation of phases, errors vary from less than $10°$ for high noise levels to less than $1°$ when the noise decreases (Figure S11-**C**). These are similar to the errors obtained with state-of-the-art methods [62–64].

An important outcome is that the same accuracy is reached with or without the assumption that the phases are equally spaced. However, challenging real data such as those acquired in a TIRF-SIM mode do benefit from the assumption that the phases are equally spaced.

Finally, let us comment on how oversampled data influence the quality of the cross-correlation map (initialization step) (Figure S11-**B**). As expected, pattern-estimation errors decrease as the oversampling increases. Yet, even with a sixteen-fold oversampling, the cross-correlation based initialization does not reach the accuracy obtained after our refinement step. This is especially true for MEP larger than 10, which corresponds to typical noise levels encountered in practice. This highlights the relevance of the proposed local refinement step.

Moreover, large oversampling factors significantly increase the memory usage and computational time. For instance, for the (512×512) image used in Figure S11, the cross-correlation computation with a sixteen-fold oversampling is six times slower than the two-step approach: initialization (with twofold oversampling) plus local refinement ($\sim$30 s vs $\sim$5 s). As such, given that exceeding a twofold oversampling for the initialization does not lead to a significant gain in the refinement step, the oversampling factor is fixed to 2 in FlexSIM.

Estimation of Pattern Low-Frequency Component. An important feature of FlexSIM is that it allows us to consider patterns of the form

$$w_m(\mathbf{x}) = \underline{w}_m(\mathbf{x}) + a_m \cos\left(\mathbf{k}^{\mathrm{t}}\mathbf{x} + \phi_m\right), \tag{5}$$

where $\underline{w}_m$ is a low-frequency component. This model proved to be crucial to obtain meaningful reconstructions for the TIRF-SIM data of Figure 2.

Regarding the estimation of $\underline{w}_m$, we deploy a simple and fast method. It relies on the fact that, given a low pass filter f, we get from (3) and (5) that

$$\begin{aligned} f * v_m &\approx f * h * (\underline{w}_m \odot u) \\ &\approx \underline{w}_m \odot (f * h * u) = \underline{w}_m \odot (f * \tilde{v}), \end{aligned} \tag{6}$$

where we recall that $\tilde{v}$ stands for the widefield image. From these approximations, we propose to use

$$\widehat{\underline{w}}_m = (f * v_m)/(f * \tilde{v}) \tag{7}$$

as an estimate of $\underline{w}_m$ (with pointwise division). This approach is illustrated in Figure S1.

B. Image Reconstruction Module

B.1. From Direct Wiener Inversion to Iterative Reconstruction Approaches. Most SIM reconstruction methods are variants of a direct Wiener inversion [2]. For standard sinusoidal

illuminations, one can easily establish and solve a closed system of equations to unmix the Fourier components of SIM data and place them back to their right location in the Fourier domain. Then, a final Wiener filtering can be used to invert the effect of the OTF and limit the amplification of noise. More evolved deconvolution approaches, for instance those that account for Poisson noise, can also be used in this final step [66]. Alternatively, the consideration of a more general variational framework allows for the use of arbitrary (non-sinusoidal) illuminations [67], a reduced number of images [68], advanced regularization terms [47, 68–70], additional out-of-focus planes in the model [47, 48], or blind reconstruction (i.e., joint pattern estimation and reconstruction) [50, 51].

B.2. Image Reconstruction with FlexSIM. We consider a variational reconstruction framework. Specifically, given P SIM raw images $\{\mathbf{y}_p \in \mathbb{R}^N\}_{p=1}^P$ composed of N pixels and associated with the (discretized) patterns $\{\mathbf{w}_p \in \mathbb{R}^N\}_{p=1}^P$, we compute the reconstructed image $\hat{\mathbf{u}} \in \mathbb{R}^{4N}$ (over a twice finer grid) as

$$\hat{\mathbf{u}} = \arg\min_{\mathbf{u}\geq 0} \sum_{p=1}^{P} \frac{1}{2}\|\mathbf{SHW}_p\mathbf{u} - \mathbf{y}_p\|^2_{\mathbf{M}_p} + \mu\mathcal{R}(\mathbf{u}), \quad \textbf{(8)}$$

where $\mathbf{S} \in \mathbb{R}^{N\times 4N}$ is a twofold (in each dimension) downsampling operator, $\mathbf{H} \in \mathbb{R}^{4N\times 4N}$ a convolution operator defined from the system PSF, and $\mathbf{W}_p = \mathbf{diag}(\mathbf{w}_p)$. Data fidelity is enforced using the "weighted" L_2-norm $\|\cdot\|^2_{\mathbf{M}_p} = \langle \mathbf{M}_p\cdot, \cdot\rangle$, where $\mathbf{M}_p \in \mathbb{R}^{N\times N}$ is defined so as to account for Poisson noise and background/out-of-focus fluorescence (details hereafter). Finally, $\mathcal{R}$ is a regularization term and $\mu > 0$ a parameter that controls the tradeoff between data fidelity and regularization.

The FlexSIM reconstruction module is implemented within the `GlobalBioIm` framework [56]. As such, a variety of regularizers $\mathcal{R}$ and optimization algorithms to solve (8) are available. By default, first-order Tikhonov, smoothed total-variation [71] and good-roughness [72] regularizers are proposed in FlexSIM. They all lead to a differentiable objective function in (8) that can be minimized through the second-order variable-metric limited-memory-bounded algorithm [73] belonging to the family of L-BFGS methods.

Weighted L_2-norm. In FlexSIM, we exploit the weighted L_2 data-fidelity term $\|\cdot\|^2_{\mathbf{M_p}}$ to account for both Poisson noise and out-of-focus fluorescence.

Poisson Noise. As in any fluorescence microscopy system, the noise in the raw SIM data is a mix of Gaussian (e.g., readout noise) and Poisson (photon-counting process of the detectors) noise. Because the associated log-likelihood is very challenging to optimize [74], standard practice is to adopt the simplifying assumption that the overall noise is a non-stationary uncorrelated Gaussian noise. This can be achieved by setting $\mathbf{M}_p = \mathbf{diag}\left(\mathbf{1}/(\mathbf{y}_p + \sigma^2)\right)$ (component-wise division), where σ^2 corresponds to the variance of the Gaussian part of the noise [69, 75].

Out-of-Focus Fluorescence. Out-of-focus fluorescence can be a source of severe reconstruction artifacts [40, 41]. To address this issue, reconstruction approaches that explicitly model and estimate the background signal have been proposed [47–49]. Another very common strategy is known as OTF attenuation [62]. It proceeds by attenuating the central frequencies of the OTF used in the Wiener-based final reconstruction. Basically, this is achieved through a pointwise multiplication of the OTF with a function of the form

$$\nu(\mathbf{k}) = 1 - \alpha\exp(-\|\mathbf{k}\|_2^2/(2\beta^2)), \quad \textbf{(9)}$$

where $\alpha > 0$ and $\beta > 0$ control the strength and the width of the attenuation, respectively. In this way, the frequency components that do not transmit any information about the missing cone are attenuated, thereby enhancing the components that can instead fill the missing cone (we refer the reader to the very instructive [62, Figure 7]). From a variational viewpoint such as (8), this OTF-attenuation strategy amounts to set $\mathbf{M}_p = \mathbf{H}_{\text{Att}}$, a convolution operator whose kernel is given in Fourier domain by ν in (9). Indeed, with this choice and setting $\mathcal{R} = \|\cdot\|_2^2$ in (8), we recover the standard Wiener-based reconstruction with OTF attenuation. This particular formulation allows us to interpret OTF attenuation as a means of giving more importance to high-frequency errors than to low-frequency errors (including errors due to the background) in the data-fidelity term.

In accordance with this section, we define in FlexSIM the data-fidelity term with $\mathbf{M}_p$ a composition of $\mathbf{diag}\left(\mathbf{1}/(\mathbf{y}_p + \sigma^2)\right)$ and $\mathbf{H}_{\text{Att}}$.

C. Sample Preparation

COS-7 cells were briefly extracted in Triton X-100/glutaraldehyde, then fixed using glutaraldehyde, before being quenched, blocked, and stained with anti-clathrin heavy-chain primary antibodies (polyclonal rabbit ab21679, abcam), revealed with donkey anti-rabbit secondary antibodies conjugated to Alexa Fluor 647, and anti-alpha tubulin primary antibodies (monoclonal mouse clones B-5-1-2 and DM1a, Sigma), revealed with donkey anti-mouse secondary antibodies conjugated to Alexa Fluor 555. To stain actin, cells were incubated with phalloidin-Atto488 at the end of the staining procedure [76].

Regarding macrophages imaging (Figure S5), macrophages were transduced with GFP-paxillin lentiviruses (BiVic facility, Toulouse, France) for three days as previously described [34]. Macrophages were fixed with paraformaldehyde and were placed on a FluoroDish (WPI FD35-100) and immersed on PBS.

D. TIRF-SIM Imaging and N-SIM Processing

We used a Nikon N-SIM-S microscope to image COS-7 cells stained for actin via classical two-beam TIRF-SIM. Cells were mounted in a Ludin chamber in 0.1M phosphate buffer. The sample was illuminated using a 488 nm laser with 2 opposite beams at the periphery of the back focal plane of a 100X, 1.49 NA objective, with 9 images (3 phases X 3 orientations; 16-bit, (1024×1024) pixels at 65 nm/pixel) captured

over a 50 ms exposure time by an Hamamatsu Fusion BT sCMOS camera. The raw images were then processed using the N-SIM module of the NIS Elements software, resulting in a 32-bit, (2048×2048) pixel reconstructed image at 32.5 nm/pixel.

E. Code Availability

The Matlab FlexSIM code is available from the GitHub repository for the project `https://github.com/esoubies/FlexSIM` In addition to the core functions of FlexSIM, this repository also contains one script per dataset of Table S1 to reproduce the results of this paper.

F. Data Availability

The scripts provided in the FlexSIM GitHub repository allow for an automatic download of the datasets listed in Table S1. The TIRF-SIM data of Figures 2, 3, S3, and S4 can be made available upon reasonable request.

Bibliography

1. Rainer Heintzmann and Christoph G. Cremer. Laterally modulated excitation microscopy: Improvement of resolution by using a diffraction grating. In *Optical Biopsies and Microscopic Techniques III*, volume 3568, pages 185–196, 1999. doi:10.1117/12.336833.
2. Mats G.L. Gustafsson. Surpassing the lateral resolution limit by a factor of two using structured illumination microscopy. *Journal of Microscopy*, 198(2):82–87, 2000. doi:https://doi.org/10.1046/j.1365-2818.2000.00710.x.
3. Rainer Heintzmann and Thomas Huser. Super-resolution structured illumination microscopy. *Chemical Reviews*, 117(23):13890–13908, 2017. doi:10.1021/acs.chemrev.7b00218.
4. Yicong Wu and Hari Shroff. Faster, sharper, and deeper: structured illumination microscopy for biological imaging. *Nature Methods*, 15(12):1011–1019, 2018. doi:https://doi.org/10.1038/s41592-018-0211-z.
5. Ying Ma, Kai Wen, Min Liu, Juanjuan Zheng, Kaiqin Chu, Zachary J. Smith, Lixin Liu, and Peng Gao. Recent advances in structured illumination microscopy. *Journal of Physics: Photonics*, 3(2):024009, 2021. doi:10.1088/2515-7647/abdb04.
6. Krishnendu Samanta and Joby Joseph. An overview of structured illumination microscopy: Recent advances and perspectives. *Journal of Optics*, 23(12):123002, 2021. doi:10.1088/2040-8986/ac3675.
7. Kirti Prakash, Benedict Diederich, Stefanie Reichelt, Rainer Heintzmann, and Lothar Schermelleh. Super-resolution structured illumination microscopy: Past, present and future. *Philosophical Transactions of the Royal Society A*, 379(2199):20200143, 2021. doi:https://doi.org/10.1098/rsta.2020.0143.
8. Lothar Schermelleh, Rainer Heintzmann, and Heinrich Leonhardt. A guide to super-resolution fluorescence microscopy. *Journal of Cell Biology*, 190(2):165–175, 2010. doi:10.1083/jcb.201002018.
9. Lothar Schermelleh, Alexia Ferrand, Thomas Huser, Christian Eggeling, Markus Sauer, Oliver Biehlmaier, and Gregor PC Drummen. Super-resolution microscopy demystified. *Nature Cell Biology*, 21(1):72–84, 2019. doi:https://doi.org/10.1038/s41556-018-0251-8.
10. Kirti Prakash, Benedict Diederich, Rainer Heintzmann, and Lothar Schermelleh. Super-resolution microscopy: A brief history and new avenues. *Philosophical Transactions of the Royal Society A*, 380(2220):20210110, 2022. doi:https://doi.org/10.1098/rsta.2021.0110.
11. Peter Kner, Bryant B Chhun, Eric R Griffis, Lukman Winoto, and Mats G.L. Gustafsson. Super-resolution video microscopy of live cells by structured illumination. *Nature Methods*, 6(5):339–342, 2009. doi:https://doi.org/10.1038/nmeth.1324.
12. Liisa M Hirvonen, Kai Wicker, Ondrej Mandula, and Rainer Heintzmann. Structured illumination microscopy of a living cell. *European Biophysics Journal*, 38:807–812, 2009. doi:https://doi.org/10.1007/s00249-009-0501-6.
13. Hui-Wen Lu-Walther, Martin Kielhorn, Ronny Förster, Aurélie Jost, Kai Wicker, and Rainer Heintzmann. FastSIM: a practical implementation of fast structured illumination microscopy. *Methods and Applications in Fluorescence*, 3(1):014001, 2015. doi:10.1088/2050-6120/3/1/014001.
14. Andreas Markwirth, Mario Lachetta, Viola Mönkemöller, Rainer Heintzmann, Wolfgang Hübner, Thomas Huser, and Marcel Müller. Video-rate multi-color structured illumination microscopy with simultaneous real-time reconstruction. *Nature Communications*, 10(1):4315, 2019. doi:https://doi.org/10.1038/s41467-019-12165-x.
15. Edward N. Ward, Lisa Hecker, Charles N. Christensen, Jacob R. Lamb, Meng Lu, Luca Mascheroni, Chyi Wei Chung, Anna Wang, Christopher J. Rowlands, Gabriele S. Kaminski Schierle, and Clemens F. Kaminski. Machine learning assisted interferometric structured illumination microscopy for dynamic biological imaging. *Nature Communications*, 13(1): 7836, 2022. doi:https://doi.org/10.1038/s41467-022-35307-0.
16. Xin Chen, Suyi Zhong, Yiwei Hou, Ruijie Cao, Wenyi Wang, Dong Li, Qionghai Dai, Donghyun Kim, and Peng Xi. Superresolution structured illumination microscopy reconstruction algorithms: a review. *Light: Science & Applications*, 12(1):172, 2023. doi:https://doi.org/10.1038/s41377-023-01204-4.
17. Pavel Křížek, Tomáš Lukeš, Martin Ovesný, Karel Fliegel, and Guy M. Hagen. SIMToolbox: a MATLAB toolbox for structured illumination fluorescence microscopy. *Bioinformatics*, 32 (2):318–320, 2015. doi:10.1093/bioinformatics/btv576.
18. Marcel Müller, Viola Mönkemöller, Simon Hennig, Wolfgang Hübner, and Thomas Huser. Open-source image reconstruction of super-resolution structured illumination microscopy data in ImageJ. *Nature Communications*, 7(1):10980, 2016. doi:https://doi.org/10.1038/ncomms10980.
19. Amit Lal, Chunyan Shan, and Peng Xi. Structured illumination microscopy image reconstruction algorithm. *IEEE Journal of Selected Topics in Quantum Electronics*, 22(4):50–63, 2016. doi:10.1109/JSTQE.2016.2521542.
20. Xiaoshuai Huang, Junchao Fan, Liuju Li, Haosen Liu, Runlong Wu, Yi Wu, Lisi Wei, Heng Mao, Amit Lal, Peng Xi, et al. Fast, long-term, super-resolution imaging with Hessian structured illumination microscopy. *Nature Biotechnology*, 36(5):451–459, 2018. doi:https://doi.org/10.1038/nbt.4115.
21. Luhong Jin, Bei Liu, Fenqiang Zhao, Stephen Hahn, Bowei Dong, Ruiyan Song, Timothy C Elston, Yingke Xu, and Klaus M Hahn. Deep learning enables structured illumination microscopy with low light levels and enhanced speed. *Nature Communications*, 11(1):1934, 2020. doi:https://doi.org/10.1038/s41467-020-15784-x.
22. Gang Wen, Simin Li, Linbo Wang, Xiaohu Chen, Zhenglong Sun, Yong Liang, Xin Jin, Yifan Xing, Yaming Jiu, Yuguo Tang, and Hui Li. High-fidelity structured illumination microscopy by point-spread-function engineering. *Light: Science & Applications*, 10(1):70, 2021. doi:https://doi.org/10.1038/s41377-021-00513-w.
23. Charles N. Christensen, Edward N. Ward, Meng Lu, Pietro Lio, and Clemens F. Kaminski. ML-SIM: universal reconstruction of structured illumination microscopy images using transfer learning. *Biomedical Optics Express*, 12(5):2720–2733, 2021. doi:10.1364/BOE.414680.
24. Zhaojun Wang, Tianyu Zhao, Huiwen Hao, Yanan Cai, Kun Feng, Xue Yun, Yansheng Liang, Shaowei Wang, Yujie Sun, Piero R. Bianco, Kwangsung Oh, and Ming Lei. High-speed image reconstruction for optically sectioned, super-resolution structured illumination microscopy. *Advanced Photonics*, 4(2):026003, 2022. doi:10.1117/1.AP.4.2.026003.
25. Gang Wen, Simin Li, Yong Liang, Linbo Wang, Jie Zhang, Xiaohu Chen, Xin Jin, Chong Chen, Yuguo Tang, and Hui Li. Spectrum-optimized direct image reconstruction of super-resolution structured illumination microscopy. *PhotoniX*, 4(1):1–18, 2023. doi:https://doi.org/10.1186/s43074-023-00092-6.
26. Chang Qiao, Di Li, Yong Liu, Siwei Zhang, Kan Liu, Chong Liu, Yuting Guo, Tao Jiang, Chuyu Fang, Nan Li, Kangmin He, Xueliang Zhu, Jennifer Lippincott-Schwartz, Qionghai Dai, and Dong Li. Rationalized deep learning super-resolution microscopy for sustained live imaging of rapid subcellular processes. *Nature Biotechnology*, 41(3):367–377, 2023. doi:https://doi.org/10.1038/s41587-022-01471-3.
27. Ruijie Cao, Yaning Li, Xin Chen, Xichuan Ge, Meiqi Li, Meiling Guan, Yiwei Hou, Yunzhe Fu, Xinzhu Xu, Christophe Leterrier, Shan Jiang, Baoxiang Gao, and Peng Xi. Open-3DSIM: an open-source three-dimensional structured illumination microscopy reconstruction platform. *Nature Methods*, 20:1–4, 2023. doi:https://doi.org/10.1038/s41592-023-01958-0.
28. Rainer Heintzmann, Thomas M. Jovin, and Christoph Cremer. Saturated patterned excitation microscopy–a concept for optical resolution improvement. *Journal of the Optical Society of America A*, 19(8):1599–1609, 2002. doi:10.1364/JOSAA.19.001599.
29. Mats G.L. Gustafsson. Nonlinear structured-illumination microscopy: Wide-field fluorescence imaging with theoretically unlimited resolution. *Proceedings of the National Academy of Sciences*, 102(37):13081–13086, 2005. doi:https://doi.org/10.1073/pnas.0406877102.
30. E. Hesper Rego, Lin Shao, John J. Macklin, Lukman Winoto, Göran A. Johansson, Nicholas Kamps-Hughes, Michael W. Davidson, and Mats G.L. Gustafsson. Nonlinear structured-illumination microscopy with a photoswitchable protein reveals cellular structures at 50-nm resolution. *Proceedings of the National Academy of Sciences*, 109(3):E135–E143, 2012. doi:https://doi.org/10.1073/pnas.1107547108.
31. Dong Li, Lin Shao, Bi-Chang Chen, Xi Zhang, Mingshu Zhang, Brian Moses, Daniel E. Milkie, Jordan R. Beach, John A. Hammer, Mithun Pasham, Tomas Kirchhausen, Michelle A. Baird, Michael W. Davidson, Pingyong Xu, and Eric Betzig. Extended-resolution structured illumination imaging of endocytic and cytoskeletal dynamics. *Science*, 349(6251):aab3500, 2015. doi:10.1126/science.aab3500.
32. Emeric Mudry, Kamal Belkebir, J. Girard, Julien Savatier, Emmeran Le Moal, C. Nicoletti, Marc Allain, and Anne Sentenac. Structured illumination microscopy using unknown speckle patterns. *Nature Photonics*, 6(5):312–315, 2012. doi:https://doi.org/10.1038/nphoton.2012.83.
33. Jérôme Idier, Simon Labouesse, Marc Allain, Penghuan Liu, Sébastien Bourguignon, and Anne Sentenac. On the superresolution capacity of imagers using unknown speckle illuminations. *IEEE Transactions on Computational Imaging*, 4(1):87–98, 2018. doi:10.1109/TCI.2017.2771729.
34. Thomas Mangeat, Simon Labouesse, Marc Allain, Awoke Negash, Emmanuel Martin, Aude Guénolé, Renaud Poincloux, Claire Estibal, Anaïs Bouissou, Sylvain Cantaloube, Elodie Vega, Tong Li, Christian Rouvière, Sophie Allart, Debora Keller, Valentin Debarnot, Xia Bo Wang, Grégoire Michaux, Mathieu Pinot, Roland Le Borgne, Sylvie Tournier, Magali Suzanne, Jérome Idier, and Anne Sentenac. Super-resolved live-cell imaging using random illumination microscopy. *Cell Reports Methods*, 1(1):100009, 2021. doi:https://doi.org/10.1016/j.crmeth.2021.100009.
35. Kévin Affannoukoué, Simon Labouesse, Guillaume Maire, Laurent Gallais, Julien Savatier, Marc Allain, Md Rasedujjaman, Loic Legoff, Jérôme Idier, Renaud Poincloux, Florence Pelletier, Christophe Leterrier, Thomas Mangeat, and Anne Sentenac. Super-resolved total internal reflection fluorescence microscopy using random illuminations. *Optica*, 10(8):1009–1017, 2023. doi:10.1364/OPTICA.487003.
36. George E. Cragg and Peter T.C. So. Lateral resolution enhancement with standing evanescent waves. *Optics Letters*, 25(1):46–48, 2000. doi:10.1364/OL.25.000046.
37. Reto Fiolka, Markus Beck, and Andreas Stemmer. Structured illumination in total internal reflection fluorescence microscopy using a spatial light modulator. *Optics Letters*, 33(14): 1629–1631, 2008. doi:10.1364/OL.33.001629.
38. Julian Roth, Johanna Mehl, and Alexander Rohrbach. Fast TIRF-SIM imaging of dynamic, low-fluorescent biological samples. *Biomedical Optics Express*, 11(7):4008–4026, 2020.

doi:10.1364/BOE.391561.
39. Yuting Guo, Di Li, Siwei Zhang, Yanrui Yang, Jia-Jia Liu, Xinyu Wang, Chong Liu, Daniel E. Milkie, Regan P. Moore, U. Serdar Tulu, Daniel P. Kiehart, Junjie Hu, Jennifer Lippincott-Schwartz, Eric Betzig, and Dong Li. Visualizing intracellular organelle and cytoskeletal interactions at nanoscale resolution on millisecond timescales. *Cell*, 175(5):1430–1442.e17, 2018. doi:https://doi.org/10.1016/j.cell.2018.09.057.
40. Justin Demmerle, Cassandravictoria Innocent, Alison J North, Graeme Ball, Marcel Müller, Ezequiel Miron, Atsushi Matsuda, Ian M Dobbie, Yolanda Markaki, and Lothar Schermelleh. Strategic and practical guidelines for successful structured illumination microscopy. *Nature Protocols*, 12(5):988–1010, 2017. doi:https://doi.org/10.1038/nprot.2017.019.
41. Christian Karras, Maria Smedh, Ronny Förster, Hendrik Deschout, Julia Fernandez-Rodriguez, and Rainer Heintzmann. Successful optimization of reconstruction parameters in structured illumination microscopy – A practical guide. *Optics Communications*, 436: 69–75, 2019. doi:https://doi.org/10.1016/j.optcom.2018.12.005.
42. Junchao Fan, Xiaoshuai Huang, Liuju Li, Shan Tan, and Liangyi Chen. A protocol for structured illumination microscopy with minimal reconstruction artifacts. *Biophysics Reports*, 5: 80–90, 2019. doi:https://doi.org/10.1007/s41048-019-0081-7.
43. Felix Kraus, Ezequiel Miron, Justin Demmerle, Tsotne Chitiashvili, Alexei Budco, Quentin Alle, Atsushi Matsuda, Heinrich Leonhardt, Lothar Schermelleh, and Yolanda Markaki. Quantitative 3D structured illumination microscopy of nuclear structures. *Nature Protocols*, 12(5):1011–1028, 2017. doi:https://doi.org/10.1038/nprot.2017.020.
44. Laurence J Young, Florian Ströhl, and Clemens F Kaminski. A guide to structured illumination TIRF microscopy at high speed with multiple colors. *JoVE (Journal of Visualized Experiments)*, (111):e53988, 2016. doi:10.3791/53988.
45. Graeme Ball, Justin Demmerle, Rainer Kaufmann, Ilan Davis, Ian M Dobbie, and Lothar Schermelleh. SIMcheck: a toolbox for successful super-resolution structured illumination microscopy. *Scientific Reports*, 5(1):15915, 2015. doi:https://doi.org/10.1038/srep15915.
46. Zhaojun Wang, Tianyu Zhao, Yanan Cai, Jingxiang Zhang, Huiwen Hao, Yansheng Liang, Shaowei Wang, Yujie Sun, Tongsheng Chen, Piero R. Bianco, Kwangsung Oh, and Ming Lei. Rapid, artifact-reduced, image reconstruction for super-resolution structured illumination microscopy. *The Innovation*, 4(3):100425, 2023. doi:https://doi.org/10.1016/j.xinn.2023.100425.
47. Emmanuel Soubies and Michael Unser. Computational super-sectioning for single-slice structured-illumination microscopy. *IEEE Transactions on Computational Imaging*, 5(2): 240–250, 2019. doi:10.1109/TCI.2018.2887136.
48. Aurélie Jost, Elen Tolstik, Polina Feldmann, Kai Wicker, Anne Sentenac, and Rainer Heintzmann. Optical sectioning and high resolution in single-slice structured illumination microscopy by thick slice blind-SIM reconstruction. *PloS One*, 10(7):e0132174, 2015. doi:https://doi.org/10.1371/journal.pone.0132174.
49. Yanquan Mo, Kunhao Wang, Liuju Li, Shijia Xing, Shouhua Ye, Jiayuan Wen, Xinxin Duan, Ziying Luo, Wen Gou, Tongsheng Chen, Yu-Hui Zhang, Changliang Guo, Junchao Fan, and Liangyi Chen. Quantitative structured illumination microscopy via a physical model-based background filtering algorithm reveals actin dynamics. *Nature Communications*, 14(1):3089, 2023. doi:10.1038/s41467-023-38808-8.
50. R. Ayuk, H. Giovannini, A. Jost, E. Mudry, J. Girard, T. Mangeat, N. Sandeau, R. Heintzmann, K. Wicker, K. Belkebir, and A. Sentenac. Structured illumination fluorescence microscopy with distorted excitations using a filtered blind-SIM algorithm. *Optics Letters*, 38 (22):4723–4726, 2013. doi:10.1364/OL.38.004723.
51. Simon Labouesse, Awoke Negash, Jérôme Idier, Sébastien Bourguignon, Thomas Mangeat, Penghuan Liu, Anne Sentenac, and Marc Allain. Joint reconstruction strategy for structured illumination microscopy with unknown illuminations. *IEEE Transactions on Image Processing*, 26(5):2480–2493, 2017. doi:10.1109/TIP.2017.2675200.
52. Emmanouil Xypakis, Giorgio Gosti, Taira Giordani, Raffaele Santagati, Giancarlo Ruocco, and Marco Leonetti. Deep learning for blind structured illumination microscopy. *Scientific Reports*, 12(1):8623, 2022. doi:https://doi.org/10.1038/s41598-022-12571-0.
53. Carlas S Smith, Johan A Slotman, Lothar Schermelleh, Nadya Chakrova, Sangeetha Hari, Yoram Vos, Cornelis W Hagen, Marcel Müller, Wiggert van Cappellen, Adriaan B Houtsmuller, Jacob P. Hoogenboom, and Sjoerd Stallinga. Structured illumination microscopy with noise-controlled image reconstructions. *Nature Methods*, 18(7):821–828, 2021. doi:https://doi.org/10.1038/s41592-021-01167-7.
54. Zafran Hussain Shah, Marcel Müller, Tung-Cheng Wang, Philip Maurice Scheidig, Axel Schneider, Mark Schüttpelz, Thomas Huser, and Wolfram Schenck. Deep-learning based denoising and reconstruction of super-resolution structured illumination microscopy images. *Photonics Research*, 9(5):B168–B181, 2021. doi:10.1364/PRJ.416437.
55. Chang Qiao, Yunmin Zeng, Quan Meng, Xingye Chen, Haoyu Chen, Tao Jiang, Rongfei Wei, Jiabao Guo, Wenfeng Fu, Huaide Lu, et al. Zero-shot learning enables instant denoising and super-resolution in optical fluorescence microscopy. *bioRxiv*, pages 2023–02, 2023. doi:https://doi.org/10.1101/2023.02.24.529803.
56. Emmanuel Soubies, Ferréol Soulez, Michael T McCann, Thanh-an Pham, Laurène Donati, Thomas Debarre, Daniel Sage, and Michael Unser. Pocket guide to solve inverse problems with GlobalBioIm. *Inverse Problems*, 35(10):104006, 2019. doi:10.1088/1361-6420/ab2ae9.
57. Florian Wernert, Satish Babu Moparthi, Jeanne Lainé, Gilles Moulay, Fanny Boroni-Rueda, Florence Pelletier, Nicolas Jullien, Sofia Benkhelifa-Ziyat, Marie-Jeanne Papandreou, Christophe Leterrier, and Stephane Vassilopoulos. The actin-spectrin submembrane scaffold restricts endocytosis along proximal axons. *bioRxiv*, 2023. doi:10.1101/2023.12.19.572337.
58. Jiaming Qian, Yu Cao, Ying Bi, Hongjun Wu, Yongtao Liu, Qian Chen, and Chao Zuo. Structured illumination microscopy based on principal component analysis. *eLight*, 3(1):4, 2023. doi:https://doi.org/10.1186/s43593-022-00035-x.
59. Kwangsung Oh and Piero R Bianco. High-speed image reconstruction for super-resolution structured illumination microscopy using facile optimization and conversion of reconstruction code in the GPU environment. In *SPIE-CLP Conference on Advanced Photonics 2023*, volume 12746, pages 12–19, 2023. doi:https://doi.org/10.1117/12.2689967.
60. Tomas Lukeš, Guy M Hagen, Pavel Křížek, Zdeněk Švindrych, Karel Fliegel, and Miloš Klíma. Comparison of image reconstruction methods for structured illumination microscopy. In *Biophotonics: Photonic Solutions for Better Health Care IV*, volume 9129, pages 607–619, 2014. doi:https://doi.org/10.1117/12.2052621.
61. Sapna A. Shroff, James R. Fienup, and David R. Williams. Phase-shift estimation in sinusoidally illuminated images for lateral superresolution. *Journal of the Optical Society of America A*, 26(2):413–424, 2009. doi:10.1364/JOSAA.26.000413.
62. Kai Wicker, Ondrej Mandula, Gerrit Best, Reto Fiolka, and Rainer Heintzmann. Phase optimisation for structured illumination microscopy. *Optics Express*, 21(2):2032–2049, 2013. doi:10.1364/OE.21.002032.
63. Kai Wicker. Non-iterative determination of pattern phase in structured illumination microscopy using auto-correlations in Fourier space. *Optics Express*, 21(21):24692–24701, 2013. doi:10.1364/OE.21.024692.
64. Ruizhi Cao, Youhua Chen, Wenjie Liu, Dazhao Zhu, Cuifang Kuang, Yingke Xu, and Xu Liu. Inverse matrix based phase estimation algorithm for structured illumination microscopy. *Biomedical Optics Express*, 9(10):5037–5051, 2018. doi:10.1364/BOE.9.005037.
65. Laurent Condat, Jérôme Boulanger, Nelly Pustelnik, Souleymen Sahnoun, and Lucie Sengmanivong. A 2-D spectral analysis method to estimate the modulation parameters in structured illumination microscopy. In *2014 IEEE 11th International Symposium on Biomedical Imaging (ISBI)*, pages 604–607, 2014. doi:10.1109/ISBI.2014.6867943.
66. Victor Perez, Bo-Jui Chang, and Ernst Hans Karl Stelzer. Optimal 2D-SIM reconstruction by two filtering steps with Richardson-Lucy deconvolution. *Scientific Reports*, 6(1):37149, 2016. doi:https://doi.org/10.1038/srep37149.
67. Tomáš Lukeš, Pavel Křížek, Zdeněk Švindrych, Jakub Benda, Martin Ovesnỳ, Karel Fliegel, Miloš Klíma, and Guy M Hagen. Three-dimensional super-resolution structured illumination microscopy with maximum a posteriori probability image estimation. *Optics Express*, 22 (24):29805–29817, 2014. doi:https://doi.org/10.1364/OE.22.029805.
68. François Orieux, Eduardo Sepulveda, Vincent Loriette, Benoit Dubertret, and Jean-Christophe Olivo-Marin. Bayesian estimation for optimized structured illumination microscopy. *IEEE Transactions on Image Processing*, 21(2):601–614, 2012. doi:10.1109/TIP.2011.2162741.
69. Jérôme Boulanger, Nelly Pustelnik, Laurent Condat, Lucie Sengmanivong, and Tristan Piolot. Nonsmooth convex optimization for structured illumination microscopy image reconstruction. *Inverse Problems*, 34(9):095004, 2018. doi:10.1088/1361-6420/aaccca.
70. Weisong Zhao, Shiqun Zhao, Liuju Li, Xiaoshuai Huang, Shijia Xing, Yulin Zhang, Guohua Qiu, Zhenqian Han, Yingxu Shang, De-en Sun, Chunyan Shan, Runlong Wu, Lusheng Gu, Shuwen Zhang, Riwang Chen, Jian Xiao, Yanquan Mo, Jianyong Wang, Wei Ji, Xing Chen, Baoquan Ding, Yanmei Liu, Heng Mao, Bao-Liang Song, Jiubin Tan, Jian Liu, Haoyu Li, and Liangyi Chen. Sparse deconvolution improves the resolution of live-cell super-resolution fluorescence microscopy. *Nature Biotechnology*, 40(4):606–617, 2022. doi:https://doi.org/10.1038/s41587-021-01092-2.
71. Jean-François Aujol. Some first-order algorithms for total variation based image restoration. *Journal of Mathematical Imaging and Vision*, 34:307–327, 2009. doi:https://doi.org/10.1007/s10851-009-0149-y.
72. Peter J Verveer, Mark J Gemkow, and Thomas M Jovin. A comparison of image restoration approaches applied to three-dimensional confocal and wide-field fluorescence microscopy. *Journal of Microscopy*, 193(1):50–61, 1999. doi:https://doi.org/10.1046/j.1365-2818.1999.00421.x.
73. Eric Thiébaut. Optimization issues in blind deconvolution algorithms. In *Astronomical Data Analysis II*, volume 4847, pages 174–183, 2002. doi:https://doi.org/10.1117/12.461151.
74. Emilie Chouzenoux, Anna Jezierska, Jean-Christophe Pesquet, and Hugues Talbot. A convex approach for image restoration with exact Poisson–Gaussian likelihood. *SIAM Journal on Imaging Sciences*, 8(4):2662–2682, 2015. doi:https://doi.org/10.1137/15M1014395.
75. Ferréol Soulez. A "learn 2D, apply 3D" method for 3D deconvolution microscopy. In *2014 IEEE 11th International Symposium on Biomedical Imaging (ISBI)*, pages 1075–1078, 2014. doi:10.1109/ISBI.2014.6868060.
76. Angélique Jimenez, Karoline Friedl, and Christophe Leterrier. About samples, giving examples: Optimized single molecule localization microscopy. *Methods*, 174:100–114, 2020. doi:https://doi.org/10.1016/j.ymeth.2019.05.008.

ACKNOWLEDGEMENTS

The authors thanks Renaud Poincloux from Institut de Pharmacologie et de Biologie Structurale in Toulouse for the preparation of the macrophage podosomes used in Figure S5. ES and TM acknowledge the support of the ANR Micro-Blind (grant ANR-21-CE48-0008) and the ANR LabEx CIMI (grant ANR-11-LABX-0040) within the French State Programme "Investissements d'Avenir". C.L. acknowledges the INP NCIS imaging facility and Nikon Center of Excellence for Neuro-NanoImaging for service and expertise, with funding from Excellence Initiative of Aix-Marseille University, A*MIDEX, a French 'Investissements d'Avenir' program (AMX-19-IET-002) through the Marseille Imaging Institute and NeuroMarseille Institute.

AUTHOR CONTRIBUTIONS

D.S. and E.S. developed the core methodology of FlexSIM with M.U. inputs. A.N. and E.S. implemented FlexSIM and made all comparisons experiments with state-of-the-art SIM reconstruction approaches. F.P. prepared COS-7 cells of Figures 2, S3 and S4. C.L. imaged these samples with the Nikon N-SIM-S system in TIRF-SIM mode. T.M. acquired the TIRF-SIM data of Figure S5 on a home-build system. E.S. made FlexSIM reconstructions of all these TIRF-SIM data. C.L., T.M., D.S., and E.S. analysed results. E.S. wrote the manuscript with inputs from all authors.

COMPETING FINANCIAL INTERESTS

The authors declare no competing interests.